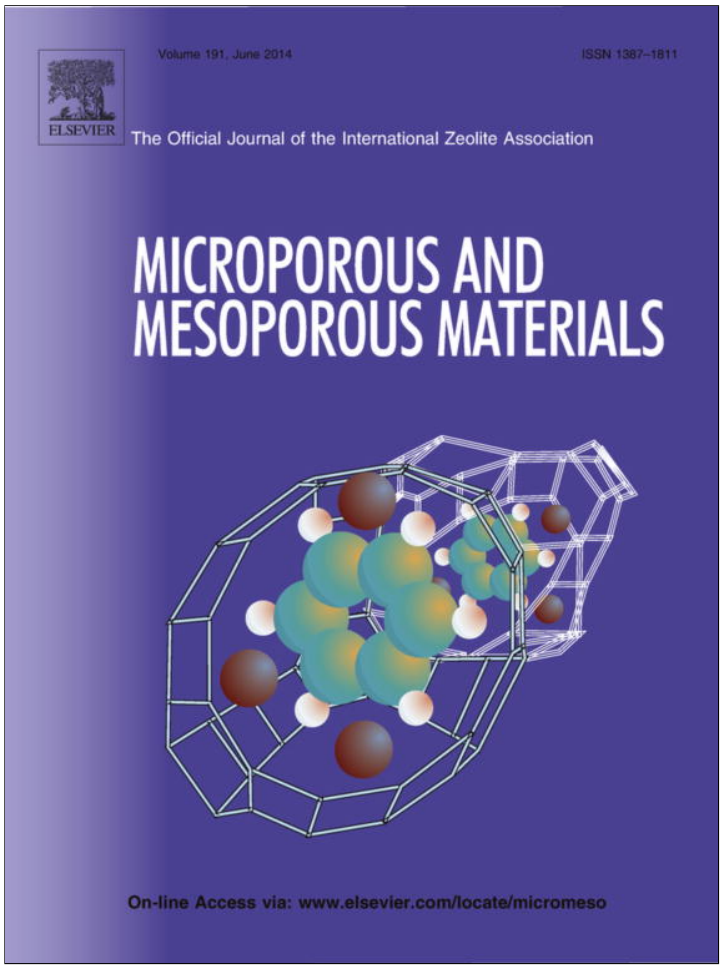

Microporous and Mesoporous Materials 191 (2014) 67–73

Contents lists available at ScienceDirect

Microporous and Mesoporous Materials

journal homepage: www.elsevier.com/locate/micromeso

Alteration of graphene based slit pores and the effect on hydrogen molecular adsorption: A simulation study

M. Georgakis *, G. Stavropoulos, G.P. Sakellaropoulos

Department of Chemical Engineering, Aristotle University of Thessaloniki, Building D, School of Engineering, University Campus, 54006, Greece

ARTICLE INFO

Article history:
Received 29 January 2013
Received in revised form 12 February 2014
Accepted 26 February 2014
Available online 6 March 2014

Keywords:
Hydrogen adsorption
Molecular Dynamics
Modification
Microporous

ABSTRACT

In this paper we investigate the effect of graphene pores' alterations on hydrogen molecular adsorption. The alterations take place in three ways: insertions at different amount of oxygen functional groups on the graphene structure, carbon atoms substitution by boron ones, and insertion of three alkyl groups. Totally one graphene pore model, six oxygenated models, two boron substituted models and three alkyl models were constructed. Hydrogen physical adsorption process was simulated via Molecular Dynamics at 77 K. Our results show that there is optimum oxygen and boron percentage for adsorption energy and gravimetric adsorption of hydrogen. On the other hand the insertion of alkyl groups leads to loss of adsorption capacity and reduction of adsorption energy for all three models.

1. Introduction

Hydrogen has been the focus of much research in the past decades, due to its potential use as a clean energy carrier. During this long time, one of the greatest obstacles for its efficient use, is the lack of an ideal storing technology for it. Different methods have been proposed and tested for its storage, such as liquefaction, compression, physical and chemical adsorption, formation of metal hydrides, etc.

All of the above have their disadvantages, namely high costs (liquefaction and metal hydrides), safety concerns (compression), lack of an ideal storage medium (adsorption). The most promising method from the above seems to be physical or chemical adsorption in solid adsorbents. Adsorption has been the subject of numerous investigations, experimental [1–33] and theoretical [34–98]. A wide range of materials have been tried and designed in the quest of the ideal storage medium, the most successful of them being activated carbons (AC) [61–65,68,70], carbon nanotubes (CNT) [64,87,88], metal organic frameworks (MOF) [7,31–33,94–100], and some curved carbonaceous structures [89–93,101,102].

Most of the experimental and theoretical works have been carried out at 77 K, whilst the adsorption of hydrogen should fulfill certain goals at room temperature. The internationally accepted goal for hydrogen gravimetric adsorption is 4.5% w/w for 2015, as set by DOE. The most important factor for a potential adsorbent is the energy of adsorption, which should be high enough to ensure satisfying gravimetric adsorption at high (room) temperatures but low enough to allow for desorption as well.

Most potential adsorbents for physical adsorption exhibit low adsorption energies, in the range 2–7 kJ/mol. The usual strategy for the enhancement of these energies is either the substitution of carbon atoms with metals (mainly) [24,59,64,66,67,73,76–78,91,96,103] or the decoration of the whole structures (with metals) [13,25,26,28,57,58,68,69,73,79,80,85,86,89,92,104], or the insertion of functional groups [29,84], or structural modification [67,105–108]. Such actions have provided some highly optimistic results especially for CNT and MOF.

This work tries to investigate the effect of a series of graphene alterations, namely carbon atoms substitution by boron ones, the insertion of oxygen functional groups at different percentages and the insertion of alkyl groups, on gravimetric adsorption and adsorption energy.

2. Simulations

All simulations and calculations took place in HyperChem, HyperCube Inc. software, on an eight-core server. The modeling work was divided into two parts: the development of the models and the set up and running of physical process simulation.

Our choice for the simulation method was Molecular Dynamics, due to the nature of physical adsorption (no bond breaking or formation). The chosen force field was the popular MM+. We present a swift presentation of the MM+ interaction equations:

Van der Waals interactions are not calculated by the standard 12-6 Lennard–Jones, but rather by:

* Corresponding author. Tel.: +30 2310 996280; fax: +30 2310 996168.
E-mail address: mgeorgak@eng.auth.gr (M. Georgakis).

http://dx.doi.org/10.1016/j.micromeso.2014.02.042
1387-1811/

$$r_{ij}^{*} = r_i^{*} + r_j^{*}$$

$$\varepsilon_{ij} = \sqrt{\varepsilon_i \varepsilon_j}$$

$$E_{\mathrm{vdW}} = \sum\nolimits_{ij \in \mathrm{vdW}} \varepsilon_{ij}(2.9 \times 10^5 \exp(-12.5\rho_{ij}) - 2.25\rho_{ij}^{-6})$$

where $\rho_{ij} = \frac{R_{ij}}{r_{ij}^{*}}$

At short distances [$r_{ij} < 3.311$] the interaction vdW equation is replaced by:

$$E_{\mathrm{vdW}} = 336.176 \sum\nolimits_{ij \in \mathrm{vdW}} \varepsilon_{ij} \varepsilon_{ij}^{-2}$$

The dihedral angle or torsional ener interaction is given by:

$$E_{\mathrm{dihedral}} = \sum_{\mathrm{dihedrals}} \frac{V1}{2}(1 - \cos 2\varphi) + \frac{V2}{2}(1 - \cos 2\varphi) + \frac{V3}{2}(1 - \cos 2\varphi)$$

The values of $V1$, $V2$, $V3$ [kcal/mol] are supplied as a Supplementary document.

Bond stretch and angle bending cross term are calculated by:

$$E_{\mathrm{stretch-bond}} = 2.51118 \sum_{\mathrm{angles}} K_{\mathrm{sb}}(\theta - \theta_0)_{ijk}[(r - r_0)_{ik} + (r - r_0)_{jk}]$$

If atom j or k is hydrogen, $r - r_0$ equals zero. In any other case, $K_{\mathrm{sb}} = 0.120$ for XR_2 and $K_{\mathrm{sb}} = 0.090$ for XRH (where X is an atom of the first row) and $K_{\mathrm{sb}} = 0.250$ for XR_2 and $K_{\mathrm{sb}} = -0.400$ for XRH (where X is an atom of the second row).

Angle bending energy is given by:

$$E_{\mathrm{bondangle}} = 0.043828 \sum_{\mathrm{angles}} \frac{1}{2} K_\theta (\theta - \theta_0)^2 [1 + \mathrm{SF}(\theta - \theta_0)^4]$$

where $\mathrm{SF} = 7 \cdot 10^{-8}$.

Dipoles interactions energy is given by:

$$E_{\mathrm{dipole}} = 14.39418\varepsilon \sum_{ij \in \mathrm{polarbonds}} \mu_i \mu_j \left[\frac{\cos x - 3 \cos a_i \cos a_j}{R_{ij}^3} \right]$$

where ε is the dielectric constant [assumed to be 1.5 in HyperChem], the angle x is the angle between the two dipole vectors and the angles a_i, a_j are the angles between the R_{ij} vector and the two dipole vectors.

Bond stretching interactions are calculated by:

$$E_{\mathrm{bond}} = 143.88 \sum_{\mathrm{bonds}} \frac{1}{2} K_r (r - r_0)^2 \times [1 + switch(r - r_0, -\frac{1}{3}\mathrm{CS}, -\frac{4}{3}\mathrm{CS})\mathrm{CS}(r - r_0)]$$

The default value for CS is −2.0 in HyperChem.

2.1. Development of the models

Hydrogen was modeled as a cloud of two-centered molecules, based on the MM+ field of molecular mechanics. Three hundred molecules were constructed in a periodic box of $56 \times 56 \times 56$ Å^3, which is the maximum allowed dimension of the used software. The cloud underwent Molecular Dynamics simulations at 77 K, until the total energy of the system presented no fluctuations. This time period of the simulations was 200 ps. During the process, the total and the kinetic energy were recorded. Multiple MD simulations provided equivalent results. Geometry optimization calculations also provided equivalent results.

The solid models were constructed in two steps. First, normal 5×5, 6×6 and 9×9 graphene sheets were constructed (number of benzoic rings per sheet) using Geometry optimization algorithms and then the substitutions took place. Geometry optimizations were based on Polak–Ribiere algorithm (conjugate gradient) with termination conditions of an RMS gradient 0.01 kcal Å^{-1} mol^{-1}. The used algorithm does not have any effect on the results of the simulation. The chosen algorithm needs logical amount of computational time to reach the asked precision. Other algorithms could be used, in a different kind of investigation, such as conformational search [larger or smaller 'jumps'].

Two models based on carbon substitution with boron were constructed, namely 16B and 32B, standing for the substitution of 16 and 32 carbon atoms on a 6×6 graphene, respectively. The new models underwent an additional geometry optimization process, with the same operating and termination conditions as mentioned above. The finalized structures and their properties are presented in Fig. 1 and Table 1, respectively.

Six oxygenated models were also constructed, as presented in Table 1 and shown in Fig. 2, by inserting different oxygen functional groups that are commonly met in AC, at different amounts in a 9×9 graphene. After the insertion of the oxygen groups, new geometry optimizations were carried out as well. The six models were named oxy1 to oxy6, and their respective oxygen gravimetric ration was set in the range 2.62% (for oxy6) to 8.38% (for oxy1). The oxy models were based on a heavier edition of a slit shaped pore, with three graphene sheets per pore wall.

The final three models (named $R1$, $R2$ and $R3$) used in this investigation resulted from the insertion of alkyls $-CH_3$, $-CH_2CH_3$ and $-CH_2CH_2CH_3$ on a 5×5 graphene sheet, in the way depicted in Fig. 3. Properties also reported in Table 1.

All twelve models were constructed under the slit pore assumption. The oxy models' walls were created by setting three parallel graphenes at 3.34 Å apart. For all models, a slit shaped pore of 7 Å was used, for comparison reasons with our previous work.

2.2. Adsorption simulations of hydrogen molecular adsorption on the altered graphene based slit pore models, at 77 K

Initially, the two systems (hydrogen cloud and a solid model) were merged into a new one, inside the same periodic box. Any hydrogen molecules that happened to be in a place inside the solid or too close to it were removed from the box. Possible presence of these molecules would lead to system explosion due to extremely high temperatures and kinetic energies.

During the MD simulations only the hydrogen molecules were allowed to move, in the stable environment of the solid. The solid models are used to create the potential energy surface (PES) of the system. The MD simulations were set up as following: the run time was set to 900 ps, which proved to be more than enough for the completion of the process. When equilibrium was achieved the simulation was terminated. The temperature was set constant at 77 K with a bath relaxation time of 0.01 ps. The MM+ field (molecular mechanics) was used throughout the simulations. Energy and its major components were recorded and graphed during the simulations. The used potential is the Lennard–Jones 12–6 potential. Hydrogen molecules are depicted as two-centered molecules.

MD simulations provide a specific advantage compared to MC ones: MD simulations provide 'real time' depiction of the physical process, in contrast to MC which provides statistical snapshots. This is important when you want to clarify a process mechanism, as in the present case.

The adsorbed quantity, the adsorption pressures, the adsorption energies were all calculated at the end of the simulations using actual calculations [no models, empirical or semi-empirical], providing high accuracy results. To be explicit:

Adsorption quantity was measured from the actual number of hydrogen molecules present in the interior of the models' pores. Adsorption energy was calculated as the difference [E[solid model + adsorbed molecules] − E[solid model] − E[initial hydrogen

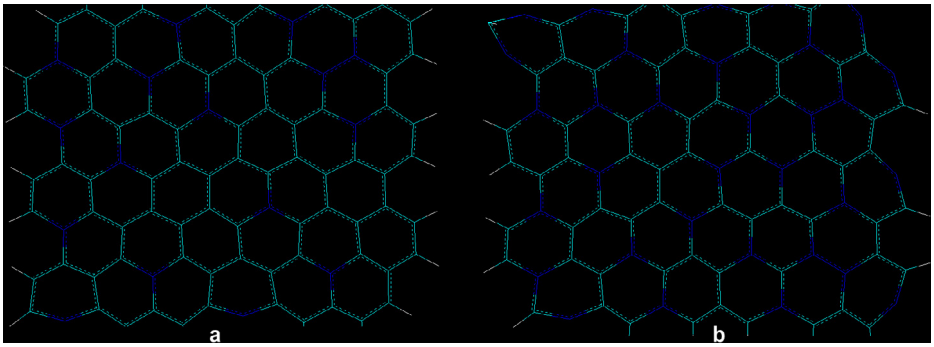

Fig. 1. (a) 16B model (b) 32B model. Boron atoms with blue. (For interpretation of the references to colour in this figure legend, the reader is referred to the web version of this article.)

Table 1
Summary of the models.

Model	Graphene size [benzoic rings]	Mass [a.u.]	Alteration
16B	6 × 6	1158	Substitution of 16 out of 96 carbon atoms with boron atoms
32B	6 × 6	1130	Substitution of 32 out of 96 carbon atoms with boron atoms
Oxy1	9 × 9	2672	Insertion of oxygen functional groups at 8.38% w/w oxygen content
Oxy2	9 × 9	2540	Insertion of oxygen functional groups at 5.67% w/w oxygen content
Oxy3	9 × 9	2494	Insertion of oxygen functional groups at 4.49% w/w oxygen content
Oxy4	9 × 9	2477	Insertion of oxygen functional groups at 3.88% w/w oxygen content
Oxy5	9 × 9	2460	Insertion of oxygen functional groups at 3.25% w/w oxygen content
Oxy6	9 × 9	2443	Insertion of oxygen functional groups at 2.62% w/w oxygen content
*R*1	5 × 5	923	Insertion of four $-CH_3$ groups in graphene (two per side)
*R*2	5 × 5	979	Insertion of four $-CH_2CH3$ groups in graphene (two per side)
*R*3	5 × 5	1035	Insertion of four $-CH_2CH_2CH_3$ groups in graphene (two per side)

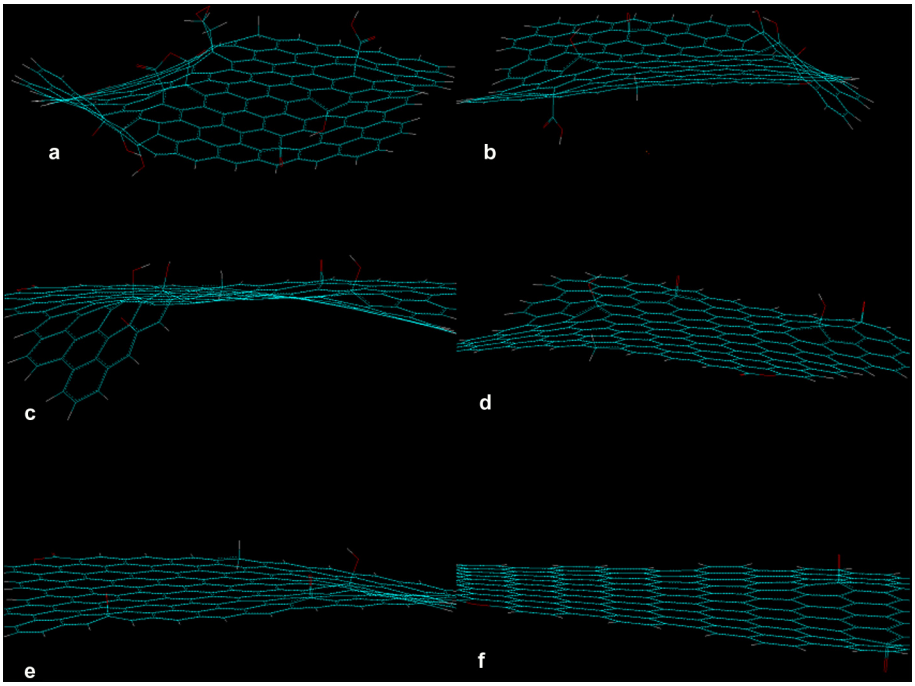

Fig. 2. The six oxygenated graphene models. Oxygen atoms with red. (For interpretation of the references to colour in this figure legend, the reader is referred to the web version of this article.)

cloud]]/[number of hydrogen molecules]. Adsorption pressures can be calculated from the number of hydrogen particles inside the periodic box but outside the solid model and the volume of the periodic box, excluding the volume of the model [using for example the Avogadro equation of state].

3. Results and discussion

Figs. 4–6 provide snapshots at the end of the adsorption process for the models used in this study. The first observation derived from these snapshots is about the planarity of the graphene

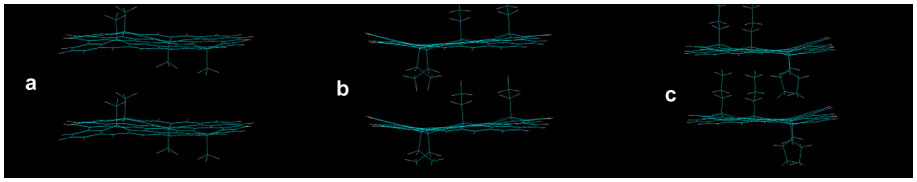

Fig. 3. Models *R*1, *R*2, *R*3.

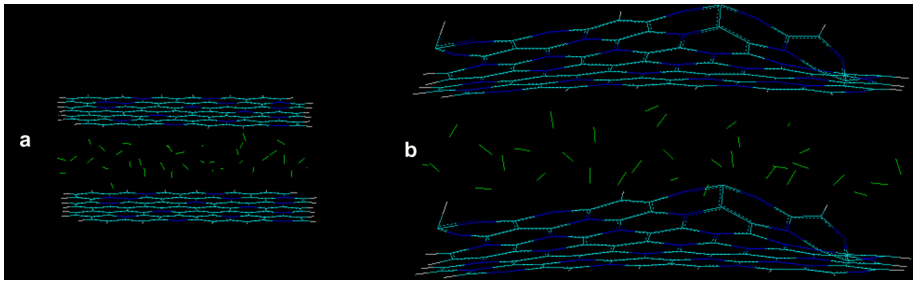

Fig. 4. Snapshots at the end of the adsorption process for (a) 16B, 7 Å pore, 77 K time 300 ps (b) 32B, 7 Å pore, 77 K, 300 ps.

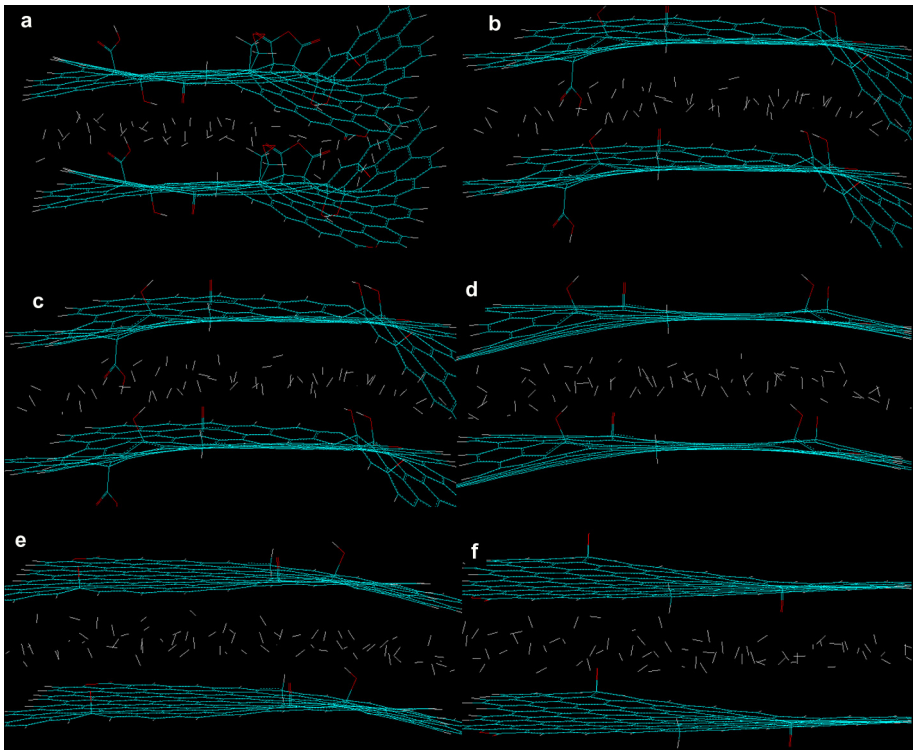

Fig. 5. Snapshots of the adsorption process for (a) oxy1 (b) oxy2 (c) oxy3 (d) oxy4 (e) oxy5 (f) oxy 6, at 77 K, 7 Å pore, 350 ps.

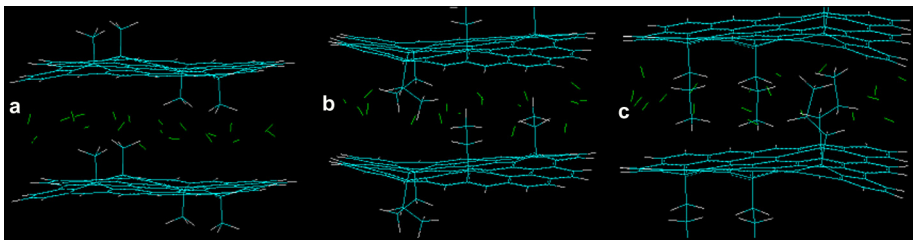

Fig. 6. Snapshots of the adsorption process. (a) *R*1, 77 K, 7 Å, 250 ps (b) *R*2, 77 K, 7 Å, 260 ps (c) *R*3, 77 K, 7 Å, 260 ps.

models. The alkyl substituted models, retain their planarity as graphene sheets with local exceptions, the oxygenated models demonstrate deviations proportional to their oxygen content, while 16B shows minor and 32B major distortions. The snapshots are taken at the end of the simulations.

Table 2 summarizes the predictions for the % gravimetric adsorption and adsorption energy for all models. It is concluded that the insertion of the alkyl groups leads to a decrease of the adsorption capacity in comparison to the initial graphene by 16.99%, 33.48% and 29.69% for *R*1, *R*2 and *R*3, respectively. On the contrary, substitution of 16 and 32 carbon atoms by boron atoms leads to an increase of the gravimetric adsorption by 19.11% and 11.81% for 16B and 32B. The oxygenated models seem to show a uniform trend for adsorption reduction with increase of oxygen content.

Comparing our work to a relative study [109] on boron doped carbon microstructures based on ab initio calculations and MC simulations, some interesting observations can be made. In the mentioned paper, the amount of boron is in the range of 5–10% [atoms] and no deviations from the planarity of the graphene structure are observed. This is in agreement with our simulations that prove that for substitutions up to 16.67% [atoms] deviations do not appear or are minor. In our second model [33.33% atoms substitution] deviations are evident. Secondly, in the mentioned paper, adsorption energies in the range of 10.5–13.0 kJ/mol are predicted, in significant agreement with our predictions of 11–13 kJ/mol. The two studies can act supplementary to each other, the mentioned one[112] for low amount of substitution [5–10%], and ours for higher amounts of substitution [16.67–33.33%], unveiling optimum areas of boron atomic substitutions.

It should be kept in mind, that the oxy models are based on a heavier version of the slit pore model, with three graphenes per wall. Removing the two graphenes per wall, leads to a new oxy3 model, that provides after a new simulation, a prediction for 2.13% w/w hydrogen adsorption at 77 K for the pore size of 7Å. This is important to notice, because it proves that the solid–fluid interactions at 77 K cannot be significantly increased by adding new graphenes (carbon atoms that is). The observed increase is mostly attributed to the reduction of the weight model (by 67%). The loss of oxygen groups seems to reduce the overall adsorption as well. The oxygen groups of the external graphenes of the walls only contribute to the total solid–fluid interaction, without presenting any steric hindrances, in contrast to the internal functional groups.

Hydrogen molecules inside the pores are in a compressed state, as it is denoted by the adsorbed densities in Table 2. This observation also reveals the obstacles for greater enhancement of adsorption in microporous carbonaceous materials, since even better hydrogen molecules rearrangement will have to be achieved in order to increase adsorption.

Adsorption energy is clearly reduced for all alkyl models in comparison to the initial graphene, but it is significantly increased for the boron substituted models. Boron insertion in the carbonaceous models demonstrates similar trends with the reported results and predictions for CNTs. The adsorption energies for 16B and 32B reached 13 and 11 kJ/mol, respectively. These values are on the upper limit of physical adsorption, as it is accepted. The oxygenated models demonstrate a possible maximum for the adsorption energy for oxy3, at 5.2 kJ/mol.

Clearly, the presence of boron atoms has led to an enhancement of solid–fluid interactions, possibly due to charges redistribution and local structural modifications. It is worth noting that the substitution of sixteen carbon atoms has led to better results both for gravimetric capacity and adsorption energy, in contrast to the case of oxy3 model, where the adsorption energy demonstrated a maximum but the gravimetric capacity did not. Possible alteration of the boron insertion scheme might provide new insight in the adsorption mechanism. In this study, boron was inserted in a uniform fashion.

A difference in the models' efficiency for hydrogen molecular adsorption is the placing of the oxygen functional groups and alkyls in the graphene pore, in contrast to the boron substitution. In the first case, because the inserted groups are protruding from the graphene layers, structural prohibitions are created. These prohibitions, reduce the effective accessible pore volume and as a consequence, the gravimetric adsorption as well. On the matter of the adsorption energy however, they do not have an effect, as the adsorption energy is a measure of solid–fluid interactions (in the case of the one graphene per wall, as discussed earlier).

It is obvious that two factors should be analyzed in order to explain the results for the adsorption in the R- and oxy-models. These factors are the increase in accessible surface which is created by the newly inserted structures and the modification in the energies of adsorption where it happens due to structural and chemical modifications. The change of the models' mass also causes a proportional change in the % w/w hydrogen adsorption, not the mechanism itself.

As discussed also elsewhere [110], these two factors act against each other in the following manner. The accessible surface area for adsorption increases for all R- and oxy- models, due to the insertion of 'fragments' in the structure of the initial graphene. This increase has a proportional positive effect on hydrogen adsorption. On the other hand, the presence of fragments causes the interaction energies to be lowered [110], thus lowering the amount adsorbed. In the case of R- models, which only consist of carbon and hydrogen atoms, the overall effect is negative [the decrease of interaction energy is more efficient than the increase of surface]. In the case of the oxy- models however, where due to the effect of oxygen functional groups on the interaction energy [especially for the models oxy-1 to oxy-4 the adsorption energies remain high, in the range 4.4–5.2 kJ/mol], the competition between the two factors is more balanced.

Table 2

Model	% w/w adsorption	Adsorption energy [kJ/mol]	Hydrogen adsorbed density [g cm^{-3}]
16B	3.11	13	0.053
32B	2.92	11	0.048
Oxy1	0.67	4.4	0.050
Oxy2	0.76	4.6	0.053
Oxy3	0.90	5.2	0.060
Oxy4	0.93	5.0	0.062
Oxy5	0.96	3.3	0.062
Oxy6	0.98	3.2	0.063
*R*1	2.17	2.3	0.047
*R*2	1.74	2.4	0.040
*R*3	1.84	2.5	0.044

To further investigate the solid–fluid interactions, we measured the closest distances between the solid and a hydrogen molecule. These distances, were found to diminish in the order: alkyl models (2.98 Å) > oxygenated models (2.91 Å) > B substituted models (2.81 Å). These distances also show where the first adsorbed layer of hydrogen molecules will form. These distances can be a quick tool for determining new models' interactions with fluids.

4. Conclusions

This work presented a multi-level investigation of the alteration of microporous carbonaceous materials, via insertion of functional groups or substitution of carbon atoms by boron ones, on the hydrogen molecular adsorption. By using Molecular Dynamics, and creating twelve solid models, we reported predictions on the gravimetric adsorption of hydrogen, the energy of adsorption and the adsorbed density of hydrogen in the solid structures.

Our predictions show that boron doping presents high potential for enhancing hydrogen adsorption at higher temperatures, due to its high energy of adsorption, which reached 13 and 11 kJ/mol for models 16B and 32B, respectively. Nevertheless, higher gravimetric adsorption at 77 K should be sought. Clearly, boron insertion increases solid–fluid interactions significantly and further improvement should be pursued. On the other hand, alkyl insertion failed at both gravimetric adsorption and adsorption energy targets, and should not be investigated any further. The insertion of oxygen functional groups provided insight into the steric hindrances that may occur during adsorption processes and a new way of insertion will be investigated in our forthcoming work.

Appendix A. Supplementary data

Supplementary data associated with this article can be found, in the online version, at http://dx.doi.org/10.1016/j.micromeso.2014.02.042.

References

[1] J.B. Parra, C.O. Ania, A. Arenillas, F. Rubiera, J.M. Palacios, J.J. Pis, Alloys Compd. 379 (2004) 280.
[2] G.X. Chen, M.H. Hong, T.S. Ong, H.M. Lam, W.Z. Chen, H.I. Elim, Carbon 42 (2004) 2735.
[3] B. Panella, M. Hircher, S. Roth, Carbon 43 (2005) 2209.
[4] A.C. Dillon, M.J. Heben, Appl. Phys. A 72 (2001) 133.
[5] R. Gadiou, S.-E. Saadallah, T. Piquero, P. David, J. Parmentier, C. Vix-Guterl, Microporous Mesoporous Mater. 79 (2005) 121.
[6] M. Jorda-Beneyto, D. Lozano-Castello, F. Suarez-Garcia, D. Cazorla-Amoros, A. Linares-Solano, Microporous Mesoporous Mater. 112 (2008) 235.
[7] V.V. Bhat, C.I. Contescu, N.C. Gallego, F.S. Baker, Carbon 48 (2010) 1331.
[8] D. Lozano-Castello, M.A. Lillo-Rodenas, D. Cazorla-Amoros, D. Linares-Solano, Carbon 39 (5) (2001) 741.
[9] M.A. Lillo-Rodenas, D. Lozano-Castello, D. Cazorla-Amoros, A. Linares-Solano, Carbon 39 (5) (2001) 751.
[10] M.A. de la Casa-Lillo, F. Lamari-Darkrim, D. Cazorla-Amoros, A. Linares-Solano, J. Phys. Chem. B 106 (42) (2002) 10930.
[11] M. Jorda-Beneyto, F. Suarez-Garcia, D. Lozano-Castello, D. Cazorla-Amoros, A. Linares-Solano, Carbon 45 (2) (2007) 293.
[12] N. Texier-Mandoki, J. Dentzer, T. Piquero, S. Saadallah, P. David, C. Vic-Guterl, Carbon 42 (12–13) (2012) 2744.
[13] Y. Li, R.T. Yang, J. Phys. Chem. C 111 (29) (2007) 11086.
[14] G. Yushin, R. Dash, J. Jagiello, J.E. Fischer, Y. Gogotsi, Adv. Funct. Mater. 16 (17) (2006) 2288.
[15] J.B. Maria, L.C. Dolores, S.G. Fabian, C.A. Diego, L.S. Angel, Microporous Mesoporous Mater. 112 (2008) 235.
[16] C.H. Chen, C.C. Huang, Int. J. Hydrogen Energy 32 (2007) 237.
[17] A. Gigras, S.K. Bhatia, A.V. Anil Kumar, A.L. Myers, Carbon 45 (2007) 1043.
[18] P. Benard, R. Chahine, P.A. Chandonia, D. Cossement, G. Dorval-Douville, L. Lafi, P. Lachance, R. Paggiaro, E. Poirier, J. Alloy. Compd. 446–447 (2007) 380.
[19] F.O. Erdogan, T. Kopac, Int. J. Hydrogen Energy 32 (2007) 3448.
[20] M. Hirscher, B. Panella, J. Alloy. Compd. 404–406 (2005) 399.
[21] Y. Zhou, K. Feng, Y. Sun, L. Zhou, Chem. Phys. Lett. 380 (2003) 526.
[22] P.A. Georgiev, D.K. Ross, P. Albers, A.J. Ramirez-Guesta, Carbon 44 (13) (2006) 2724.
[23] A. Centrone, L. Brambilla, G. Zerbi, Phys. Rev. B 71 (24) (2005) 245406.
[24] Z. Zheng, Q. Gao, J. Jiang, Carbon 48 (10) (2010) 2968–2973.
[25] C.C. Huang, H.M. Chen, C.H. Chen, Int. J. Hydrogen Energy 35 (2010) 2777.
[26] K.Y. Kang, B.I. Lee, J.S. Lee, Carbon 47 (4) (2009) 1171–1180.
[27] X.C. Xu, K. Takahashi, Y. Matsuo, Y. Hattori, M. Kumagai, S. Ishiyama, K. Kaneko, S. Iijima, Int. J. Hydrogen Energy 32 (2007) 2504.
[28] Y.X. Yang, L. Bourgeois, C. Zhao, D. Zhao, A. Chaffee, P.A. Webley, Microporous Mesoporous Mater. 119 (2009) 36–46.
[29] S.K. Beyaz, F. Darkrim Lamari, B.P. Weinberger, P. Gadelle, L. Firlej, P. Bernier, Int. J. Hydrogen Energy 34 (2009) 1965.
[30] N. Nishimiya, K. Ishigaki, H. Takikawa, M. Ikeda, Y. Hibi, T. Sakakibara, et al., J. Alloys Compd. 339 (2002) 275.
[31] D. Saha, Z. Wei, S. Deng, Int. J. Hydrogen Energy 33 (2008) 7479.
[32] D. Saha, S. Deng, Int. J. Hydrogen Energy 34 (2009) 2670.
[33] S.S. Kaye, A. Dailly, O.M. Yaghi, J.R. Long, J. Am. Chem. Soc. 129 (2007) 14176.
[34] D.D. Do, S. Junpirom, D. Nicholson, H.D. Do, Aspects 353 (2010) 10–29.
[35] K.V. Kumar, M.M. de Castro, M. Martinez-Escandell, M. Molina-Sabio, F. Rodriguez-Reinoso, Chem. Eng. J. 159 (2010) 272–279.
[36] K. Wang, J.K. Johnson, Mol. Phys. 95 (1998) 299.
[37] K. Wang, J.K. Johnson, J. Chem. Phys. 110 (1999) 577.
[38] K. Wang, J.K. Johnson, J. Phys. Chem. B 103 (1999) 277.
[39] K. Wang, J.K. Johnson, J. Phys. Chem. B 103 (1999) 4809.
[40] V.V. Simonyan, P. Diep, J.K. Johnson, J. Chem. Phys. 111 (1999) 9778.
[41] F. Darkrim, D. Levesque, J. Chem. Phys. 109 (1998) 4981.
[42] M. Rzepka, P. Lamp, M.A. de la-Casa Lillo, J. Phys. Chem. B 102 (1998) 10894.
[43] P.A. Gordon, R.B. Saeger, Ind. Eng. Chem. Res. 38 (1999) 4647.
[44] Y. Yin, B. McEnaney, T. Mays, Langmuir 16 (2000) 10521.
[45] H.S. Chen, G. Pez, G. Kern, G. Kress, J. Hafner, J. Phys. Chem. B 105 (2001) 736.
[46] A.S. Claye, J.E. Fischer, Electrochem. Acta 45 (1999) 107.
[47] A. Touzik, H. Hermann, Chem. Phys. Lett. 416 (2005) 137.
[48] L. Zhang, K. Li, X. Zhu, C. Lv, L. Ling, Carbon 40 (2002) 445.
[49] V.K.H. Dobruskin, Carbon 40 (2002) 659.
[50] J. Jagiello, M. Thommes, Carbon 42 (2004) 1227.
[51] D.D. Do, H.D. Do, Langmuir 20 (2004) 7103.
[52] S. Challet, P. Azais, R.J.-M. Pellenq, O. Isnard, J.-L. Soubeyroux, L. Duclaux, J. Phys. Chem. Solids 65 (2004) 541.
[53] S.K. Bhatia, K. Tran, T.X. Nguyen, D. Nicholson, Langmuir 20 (2004) 9612.
[54] M.J. Biggs, A. Buts, D. Williamson, Langmuir 20 (2004) 5786.
[55] R.C. Aga, C.L. Fu, M. Krcmar, J.R. Morris, Phys. Rev. B 76 (16) (2007) 165404.
[56] I. Cabria, M.J. Lopez, J.A. Alonso, Carbon 45 (13) (2007) 2649.
[57] I. Cabria, M.J. Lopez, J.A. Alonso, J. Chem. Phys. 123 (20) (2005) 204721.
[58] R.J.M. Pellenq, F. Marinelli, J.D. Fuhr, F. Fernadez-Alonso, K. Refson, J. Chem. Phys. 129 (22) (2008) 224701.
[59] Z. Yang, Y. Xia, R. Mokaya, J. Am. Chem. Soc. 129 (2007) 1673.
[60] E. Garrone, B. Bonelli, C. Otero Arean, Chem. Phys. Lett. 456 (2008) 68.
[61] Z. Zhou, X. Gao, J. Yan, D. Song, Carbon 44 (5) (2006) 939.
[62] Z. Zhou, J. Zhao, Z. Chen, X. Gao, T. Yan, B. Wen, et al., J. Chem. Phys. B 110 (2006) 13363.
[63] Z.H. Zhu, H. Hatori, S.B. Wang, G.Q. Lu, J. Phys. Chem. B 109 (2005) 16744.
[64] M. Sankaran, B. Viswanathan, Carbon 44 (2006) 2816.
[65] Z. Yang, Y. Xia, X. Sun, R. Mokaya, J. Phys. Chem. B 110 (2006) 18424.
[66] M.C. Nguyen, H. Lee, J. Ihm, Solid State Commun. 147 (2008) 419.
[67] B. Kuchta, L. Firlej, S. Roszak, P. Pfeifer, C. Wexler, Appl. Surf. Sci. 256 (2010) 5270–5274.
[68] Z.M. Ao, T.T. Tan, S. Li, Q. Jiang, Solid State Commun. 149 (2009) 1363.
[69] Q. Sun, P. Jena, Q. Wang, M. Marquez, J. Am. Chem. Soc. 128 (2006) 9741.
[70] B. Kuchta, L. Firlej, P. Pfeifer, C. Wexler, Carbon 48 (2010) 223.
[71] S.K. Bhatia, A.L. Myers, Langmuir 22 (4) (2006) 1688.
[72] D.Y. Sun, J.W. Liu, X.G. Gong, Z.F. Liu, Phys. Rev. B 75 (2007) 075424.
[73] H.L. Park, S.C. Yi, Y.C. Chung, Int. J. Hydrogen Energy 35 (2010) 3583.
[74] C. Ataca, E. Akturk, S. Ciraci, Phys. Rev. B 79 (2009) 041406.
[75] G. Kim, S.H. Jhi, N. Park, S.G. Louie, M.L. Cohen, Phys. Rev. B 78 (2008) 085408.
[76] B. Kuchta, L. Firlej, R. Cepel, P. Pfeifer, C. Wexler, Aspects 357 (2010) 61.
[77] Q. Dong, W.Q. Tian, D.L. Chen, C.C. Sun, Int. J. Hydrogen Energy 34 (2009) 5444.
[78] N.S. Venkataramanan, M. Khazaei, R. Sahara, H. Mizuseki, Y. Kawazoe, Chem. Phys. 359 (2009) 173.
[79] G.E. Froudakis, Nano Lett. 1 (10) (2001) 531.
[80] G.E. Froudakis, Nano Lett. 1 (4) (2001) 179.
[81] F. Huarte-Larranga, M. Alberti, Chem. Phys. Lett. 445 (2007) 227.
[82] K. Iyakutti, Y. Kawazoe, M. Rajarajeswari, V.J. Surya, Int. J. Hydrogen Energy 34 (2009) 370.
[83] M. Georgakis, G. Stavropoulos, G.P. Sakellaropoulos, Int. J. Hydrogen Energy 32 (2007) 1999.
[84] M. Georgakis, G. Stavropoulos, G.P. Sakellaropoulos, Int. J. Hydrogen Energy 32 (2007) 3465.
[85] T. Yildirim, S. Ciraci, Phys. Rev. Lett. 94 (2005) 175501.
[86] E. Durgun, S. Ciraci, T. Yildirim, Phys. Rev. B 77 (2008) 085405.
[87] A. Zolfaghari, P. Pourhossein, H.Z. Jooya, Int. J. Hydrogen Energy 36 (2011) 13250–13254.
[88] S. Agnihotri, J.P.B. Mota, M. Rostam-Abadi, M.J. Rood, Carbon 44 (2006) 2376.
[89] N. Naghshineh, M. Hashemianzadeh, Int. J. Hydrogen Energy 34 (2009) 2319.
[90] A. Gotzias, H. Heiberg-Andersen, M. Kainourgiakis, T. Steriotis, Appl. Surf. Sci. 256 (2010) 5226–5231.
[91] G. Chen, Q. Peng, H. Mizuseki, Y. Kawazoe, Comput. Mater. Sci. 49 (2010) S378–S382.
[92] S. Banerjee, C.G.S. Pillai, C. Majumder, Int. J. Hydrogen Energy 36 (2011) 4976.

[93] V. Gayathri, N.R. Devi, R. Geetha, Int. J. Hydrogen Energy 35 (2010) 1313.
[94] D. Kim, D.H. Jung, S.B. Choi, J.H. Joon, J. Kim, K. Choi, S.H. Choi, J. Phys. Chem. Solids 69 (2008) 1428.
[95] B. Assfour, G. Seifert, Int. J. Hydrogen Energy 34 (2009) 8135.
[96] X. Zou, M.H. Cha, S. Kim, M.C. Nguyen, G. Zhou, W. Duan, J. Ihm, Int. J. Hydrogen Energy 35 (2010) 198.
[97] Y. Li, Y. Liu, Y. Wang, Y. Leng, L. Xie, X. Li, Int. J. Hydrogen Energy 32 (2007) 3411.
[98] D. Dubbeldam et al., Fluid Phase Equilib. 261 (2007) 152.
[99] M. Eddaoudi, H. Li, O.M. Yaghi, J. Am. Chem. Soc. 122 (7) (2000) 1391.
[100] B. Xiao, Q. Yuan, Particuology 7 (2009) 129.
[101] H. Heiberg-Andersen, A.T. Skjeltorp, J. Math. Chem. 42 (2007) 707.
[102] H. Heiberg-Andersen, A.T. Skjeltorp, K. Sattler, J. Non-Cryst. Solids 354 (2008) 5247.
[103] M. Sankaran, B. Viswanathan, Carbon 45 (2007) 1628.
[104] P. Chen, X. Wu, J. Lin, K.L. Tan, Science 285 (1999) 91.
[105] A. Hashimoto, K. Suenaga, A. Gloter, K. Urita, S. Iijima, Nature 430 (2004) 870.
[106] A. Lu, B.C. Pan, Phys. Rev. Lett. 92 (2004) 105504.
[107] A.J. Stone, D.J. Wales, Chem. Phys. Lett. 128 (1986) 501.
[108] M.B. Nardelli, B.I. Yakobson, J. Bernholc, Phys. Rev. Lett. 81 (1998) 4656.
[109] L. Firlej et al., J. Chem. Phys. 131 (2009) 164702.
[110] B. Kuchta et al., JACS 134 (2012) 15130.